# Electron-vibration entanglement in the Born-Oppenheimer description of chemical reactions and spectroscopy

**Laura K. McKemmish[ab], Ross H. McKenzie[c], Noel S. Hush[ad], and Jeffrey R. Reimers[ef]***

***Received (in XXX, XXX) Xth XXXXXXXXX 20XX, Accepted Xth XXXXXXXXX 20XX***
**DOI: 10.1039/b000000x**

Entanglement is sometimes regarded as the quintessential measure of the quantum nature of a system and its significance for the understanding of coupled electronic and vibrational motions in molecules has been conjectured. Previously, we considered the entanglement developed in a spatially localized *diabatic* basis representation of the electronic states, considering design rules for qubits in a low-temperature chemical quantum computer. We extend this to consider the entanglement developed during high-energy processes. We also consider the entanglement developed using *adiabatic* electronic basis, providing a novel way for interpreting effects of the breakdown of the Born-Oppenheimer (BO) approximation. We consider: (i) BO entanglement in the ground-state wavefunction relevant to equilibrium thermodynamics, (ii) BO entanglement associated with low-energy wavefunctions relevant to infrared and tunneling spectroscopies, (iii) BO entanglement in high-energy eigenfunctions relevant to chemical reaction processes, and (iv) BO entanglement developed during reactive wavepacket dynamics. A two-state single-mode diabatic model descriptive of a wide range of chemical phenomena is used for this purpose. The entanglement developed by BO breakdown correlates simply with the diameter of the cusp introduced by the BO approximation, and a hierarchy appears between the various BO-breakdown correction terms, with the first-derivative correction being more important than the second-derivative correction which is more important than the diagonal correction. This simplicity is in contrast to the complexity of BO-breakdown effects on thermodynamic, spectroscopic, and kinetic properties. Further, processes poorly treated at the BO level that appear adequately treated using the Born-Huang adiabatic approximation are found to have properties that can *only* be described using a non-adiabatic description. For the entanglement developed between diabatic electronic states and the nuclear motion, qualitatively differently behavior is found compared to traditional properties of the density matrix and hence entanglement provides new information about system properties. For chemical reactions, this type of entanglement simply builds up as the transition-state region is crossed. It is robust to small changes in parameter values and is therefore more attractive for making quantum qubits than is the related fragile ground-state entanglement, provided that coherent motion at the transition state can be sustained.

## 1. Introduction

Entanglement has been extensively researched in recent years and provides an intrinsic measure of the quantum nature of multi-particle systems.[1] The entanglement between two subsystems is zero if their dynamics are independent of one another. The entanglement is large in states that contain non-classical correlations, such as those seen in experiments in which Bell's inequalities are violated. In chemical applications, entanglement has been studied considering e.g., electron-vibration,[2-15] electron-electron,[16-29] vibration-vibration,[30-41] vibration-rotation,[42, 43] rotation-rotation,[44] and electron-spin[45-49] interactions. The primary motivation for this research has been the possibility of exploiting entanglement to fabricate a quantum information processing device with performance properties far in excess of those using classical electronics or optics.[50] A second motivation is to develop new computational quantum chemistry methods for highly correlated systems.[51] Another less explored reason for considering quantum entanglement within chemical systems is the possibility that it could provide new insight into the quantum world of molecular spectroscopy, thermodynamics, and kinetics, and indeed this aspect is currently receiving significant attention.[6, 30, 31, 52-54] Previously we have investigated low-energy electron-vibration processes for use in quantum information processing,[2, 3] and here we extend this work to higher-energy processes. However, we are also concerned with what entanglement can tell us about chemical reactions and spectroscopic processes, focusing not only the results that conceivable experiments may yield but also on the understanding of the breakdown of the Born-Oppenheimer (BO) and Born-Huang (BH) adiabatic approximations.[55-58]

The BO approximation leads to the critical concept of molecular potential-energy surfaces obtained considering the electronic motion at fixed nuclear configurations. This approach therefore neglects the effects of nuclear motion on the electronic structure, effects that give rise to unexpected chemical reaction mechanisms and to quantitative changes in molecular vibration frequencies and heats of formation.[55-58] While unexpected reaction mechanisms are of fundamental importance, our recent review[59] indicates that modern computational methods have

advanced to the stage that inclusion of this coupling is required also for the quantitative prediction of observed spectroscopic and thermodynamic properties. Some effects of BO breakdown are expensive to calculate and are implemented in only a few computational packages, but if only pairs of states are assumed to simultaneously interact, then all required terms may be evaluated from results now available in many wavefunction-based and density-functional based packages.[59-62]

Usually the accuracy of the BO approximation is gauged by the magnitude of its effects on thermochemical, spectroscopic, and kinetics processes. However, we have noted a significant caveat. While it is normal to describe unanticipated reactions as being "nonadiabatic", we have recently shown that BH adiabatic potential-energy surfaces typically describe thermally activated processes of this type quite well and hence these reactions should actually only be described as being "non-Born-Oppenheimer" ones.[59] When BH surfaces become inappropriate, dynamics intrinsically involves more than one potential-energy surface and is therefore intrinsically quantum.

A simple example that highlights all of the effects to be considered is the dissociation of the NaCl dimer in the gas phase.[63] At its equilibrium bond length, this molecule is ionic $Na^+$–$Cl^-$ but it dissociates into radicals $Na^\bullet + Cl^\bullet$.[64] The process is naively thought to happen on the ground-state BO adiabatic surface, the bonding changing continuously from essentially ionic at short distance to purely radical at long distance. However, an excited-state surface is also involved with the opposite ionic/radical character to the ground state, and the reaction really involves an avoided crossing between these two surfaces. Hence the accurate treatment of the dissociation process requires inclusion of the effects of BO breakdown, mixing the two electronic states. This mixing entangles the electronic-vibrational wavefunctions in a way that dissociation on the pure ground-state surface does not. We use this entanglement as a quantitative measure of the effects of BO breakdown.

Instead of using the BO description to understand the dissociation of the NaCl molecule, an alternative approach is to use *diabatic* wavefunctions, wavefunctions that are either *purely ionic* or *purely radical* with unchanging character as the molecule stretches. These diabatic wavefunctions are mixed in different proportions at each nuclear geometry to make the BO adiabatic wavefunctions. A particularly relevant aspect of the diabatic approach is that it is possible to build spatially localized detectors for the charge or dipole of a molecule as it undergoes dynamics, and these detectors project the quantum wavefunction onto diabatic bases. The entanglement developed in a diabatic basis can therefore conceivably be used in a quantum information processor.[4-9]

Regardless of which way we chose to represent it, all chemical reactions generate some degree of entanglement between the nuclear and electronic motions. What happens at high energy on molecular potential energy surfaces also affects low energy properties like the nature of the ground state and the lowest vibrational levels, however, as molecular properties are holistic. So for example the entanglement developed between electronic motion on the BO surfaces and the vibrations must become large during NaCl dissociation as the wavefunctions at some point display equal radical and ionic character, but even at the equilibrium geometry the wavefunction has some covalent character and hence a small amount of entanglement must remain. Previously we have shown the electron-vibration entanglement that is developed in diabatic bases for low-energy states is inappropriate for use in quantum information processing,[3] hence our interest here in higher-energy processes.

As the BO approximation is a mathematical construct, it is difficult to envisage an experiment that could perform the related measurements. However, owing to the fundamental importance of the BO approximation to the conceptual framework of chemistry, understanding this entanglement could yield conceptual advances. Indeed, this possibility is of considerable current interest,[6, 30, 31, 52, 53] as is the possibility of examining vibration-vibration entanglement resulting from BO breakdown.[30, 31] As classical molecular dynamics simulations based on the BO approximation do not allow for entanglement, the measures we provide may lead to a robust method for accessing the suitability of molecular dynamics applications to chemical kinetics and spectroscopy.

The simplest appropriate model system is the two-state one-mode vibronic coupling model (sometimes known as the two-site Holstein model[65]) in which two diabatic states (representing reactants and products) are coupled through a single harmonic-oscillator vibration. This is the approach we take.

A very wide range of chemical processes can be described using this model, and we consider in detail ten model chemical systems **0 – 9** and nine iconic parameter sets **A – I** as described in Fig. 1 and Table 1. These model systems include the origin of aromaticity in benzene,[66] symmetry breaking to produce $sp^3$ hybridization in ammonia,[66, 67] loss of aromaticity in the lowest triplet excited state of pyridine ($^3$PYR),[68] symmetry breaking in BNB, [69] intervalence charge transfer in the Creutz-Taube ion (CT)[70], its orthomethoxy substituted variant CT-OMe[71] and extended bipyridyl form DPP,[72, 73] the photosynthetic bacteriochlorophyll special-pair radical cation from *Rhodobacter sphaeroides*,[74, 75] charge recombination in a ferrocene-porphyrin-fullerene triad photosynthetic model compound ($FcPC_{60}$),[76, 77] and hole transport through the molecular conductor Alq3.[78 79]

A limitation is that this model includes only a single nuclear coordinate and hence cannot describe Jahn-Teller interactions at conical intersections that are important for in particular photochemistry. Under such circumstances, the vibronic coupling strength becomes strongly dependent on a second nuclear coordinate and the Berry Phase becomes an important property. Entanglement in these systems is also of current interest, however.[2, 10, 11]

## 2. Methods

All mathematical symbols used are compared and contrasted in the Appendix.

### a. The two-state one-mode model Hamiltonian

The model Hamiltonian **H** is written in terms of spatially localized crude-adiabatic (CA) diabatic states $\left|\phi_L^{CA}(r,Q_0)\right\rangle$ and $\left|\phi_R^{CA}(r,Q_0)\right\rangle$ as

$$\mathbf{H}^{CA}(Q)=\begin{bmatrix} H_{LL}^{CA}(Q) & H_{LR}^{CA}(Q) \\ H_{RL}^{CA}(Q) & H_{RR}^{CA}(Q) \end{bmatrix} \text{ where} \qquad (1)$$

$$H_{LL}^{CA}(Q)=\left\langle \phi_L^{CA}(r,Q_0)\middle|\mathbf{H}\middle|\phi_L^{CA}(r,Q_0)\right\rangle = \frac{\hbar\omega}{2}\left(Q+Q_m\right)^2-\frac{\hbar\omega}{2}\frac{d^2}{dQ^2}$$

$$H_{RR}^{CA}(Q)=\left\langle \phi_R^{CA}(r,Q_0)\middle|\mathbf{H}\middle|\phi_R^{CA}(r,Q_0)\right\rangle = \frac{\hbar\omega}{2}\left(Q-Q_m\right)^2-\frac{\hbar\omega}{2}\frac{d^2}{dQ^2} + E_0$$

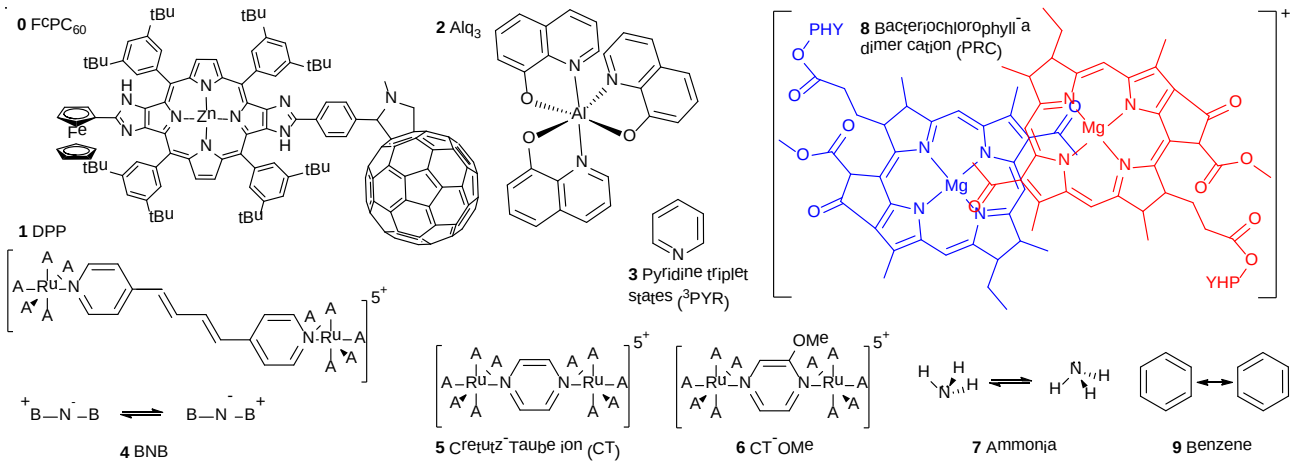


**Fig. 1** Some sample molecular systems (see text) with electronic states that can be described using two coupled diabatic potential-energy surfaces. OMe is methoxy, PHY is phytyl; $^t$Bu is tertiary butyl; A is ammonia; $FcPC_{60}$ is Zinc, [[5,10,16,21-tetrakis[3,5-bis(1,1-dimethylethyl)phenyl]-13-[4-(1',5'-dihydro-1'-methyl-2'*H*-[5,6]fullereno-$C_{60}$-$I_h$-[1,9-*c*]pyrrol-2'-yl)phenyl]-1,12-dihydro-23*H*,25*H*-diimidazo[4,5-*b*:4',5'-*l*]porphin-2-yl-κ$N^{23}$,κ$N^{24}$,κ$N^{25}$,κ$N^{26}$]ferrocenato(2-)]-, (*SP*-4-1); Alq3 is *mer*-tris(8-hydroxyquinolinato)aluminum(III); DPP is Ruthenium(5+), decaammine[μ-[4,4'-[(1*E*,3*E*)-1,3-butadiene-1,4-diyl]bis[pyridine-κ*N*]]]di- (9CI).

**Table 1** Estimates (see text) of parameters values for the coupled harmonic potential-energy surfaces for molecular systems **0** – **9** (see Fig. 1) and characteristic points **A** – **I**, along with the evaluated properties at $N$=1024: $Q_c$ - the cusp diameter (Eqn. (19)), $\Delta\Delta E^{\dagger}$ is the DC to the activation energy (Eqn. (20)); for eigenstates $\rho$ are density-matrix elements (Eqn. (12)) while $S$ is the entanglement (Eqn. (14) for the lowest vibronic level (0), first-excited level (1), and level at the transition state ($T$); for wavepackets $S_\pi$ is the entanglement at $t=\pi/\omega$ whilst $\kappa_{LR}$ gives the probability of reaction between the diabatic states per period of motion evaluated using the full Hamiltonian (FC) and its BO or BH approximations. All entanglements are in the BO basis and hence reflect the accuracy of the BO approximation rather than the usefulness of the molecules in a quantum information processor.

| System | $\frac{2\lvert J\rvert}{\lambda}$ | $\frac{\hbar\omega}{\Delta E}$ | $\frac{E_0}{\hbar\omega}$ | $Q_c$ | $\frac{\Delta\Delta E^{\dagger}}{\hbar\omega}$ | $\rho_0^{+-}$ | $\rho_0^{++}$ | $S_0$ | $\rho_1^{+-}$ | $\rho_1^{++}$ | $S_1$ | $\rho_T^{+-}$ | $\rho_T^{++}$ | $S_T$ | $S_\pi$ | $\kappa_{LR}^{FC}$ | $\kappa_{LR}^{BO}$ | $\kappa_{LR}^{BH}$ |
|---|---|---|---|---|---|---|---|---|---|---|---|---|---|---|---|---|---|---|
| **0** $FcPC_{60}$ | 0.029 | 0.15 | -13 | 0.05 | 44 | 0.000 | 0.000 | 0.000 | 0.000 | 0.000 | 0.000 | | | | | 0.02[b] | 0 | 0 |
| **1** DPP | 0.043 | 0.08 | 0 | 0.11 | 11 | 0.000 | 0.000 | 0.001 | 0.000 | 0.000 | 0.005 | 0.000 | 0.037 | 0.227 | 0.98 | 0.08 | 0.64 | 0.22 |
| **2** Alq3 | 0.08 | 0.16 | 0 | 0.14 | 6.3 | 0.000 | 0.002 | 0.020 | 0.000 | 0.009 | 0.076 | 0.000 | 0.064 | 0.344 | 0.62 | 0.11 | 0.68 | 0.27 |
| **3** $^3$PYR | 0.3 | 0.095 | 1.3[a] | 0.67 | 0.28 | 0.013 | 0.000 | 0.000 | 0.013 | 0.001 | 0.008 | 0.007 | 0.003 | 0.033 | 0.19 | 0.55 | 0.62 | 0.56 |
| **4** BNB | 0.74 | 0.18 | 0 | 1.11 | 0.10 | 0.000 | 0.001 | 0.010 | 0.000 | 0.005 | 0.041 | 0.000 | 0.001 | 0.010 | 0.04 | 0.86 | 0.92 | 0.88 |
| **5** CT | 0.80 | 0.089 | 0 | 1.68 | 0.04 | 0.000 | 0.000 | 0.002 | 0.000 | 0.001 | 0.006 | 0.000 | 0.000 | 0.002 | 0.01 | 0.80 | 0.83 | 0.81 |
| **6** CT-OMe | 0.80 | 0.089 | 1.5[a] | 1.68 | 0.04 | 0.010 | 0.000 | 0.000 | 0.019 | 0.000 | 0.001 | | | | | | | |
| **7** $NH_3$ | 0.80 | 0.006 | 0 | 6.45 | 0.003 | 0.000 | 0.000 | 0.000 | 0.000 | 0.000 | 0.000 | 0.000 | 0.000 | 0.000 | 0.00 | 0.50 | 0.50 | 0.50 |
| **8** PRC | 1.8 | 0.41 | 0.6 | 1.39 | 0.07 | 0.020 | 0.003 | 0.023 | 0.040 | 0.016 | 0.108 | | | | | | | |
| **9** Benzene | 3.3 | 0.010 | 0 | 12.6 | 0.001 | 0.000 | 0.000 | 0.000 | 0.000 | 0.000 | 0.000 | | | | | | | |
| **A** | 0.1 | 1 | 0 | 0.07 | 25 | 0.000 | 0.101 | 0.471 | 0.000 | 0.212 | 0.746 | 0.000 | 0.212 | 0.746 | 0.31 | 0.05 | 0.76 | 0.26 |
| **B** | 1 | 1 | 0 | 0.59 | 0.35 | 0.000 | 0.024 | 0.161 | 0.000 | 0.242 | 0.799 | | | | | | | |
| **C** | 10 | 1 | 0 | 2.23 | 0.025 | 0.000 | 0.005 | 0.044 | 0.000 | 0.332 | 0.917 | | | | | | | |
| **D** | 0.01 | 0.1 | 0 | 0.02 | 250 | 0.000 | 0.000 | 0.003 | 0.000 | 0.000 | 0.005 | 0.000 | 0.017 | 0.122 | 0.81 | 0.02 | 0.67 | 0.02 |
| **E** | 0.1 | 0.1 | 0 | 0.22 | 2.5 | 0.000 | 0.000 | 0.001 | 0.000 | 0.001 | 0.015 | 0.000 | 0.051 | 0.289 | 0.86 | 0.24 | 0.64 | 0.39 |
| **F** | 1 | 0.1 | 0 | 1.88 | 0.035 | 0.000 | 0.000 | 0.002 | 0.000 | 0.001 | 0.007 | | | | | | | |
| **G** | 10 | 0.1 | 0 | 7.05 | 0.003 | 0.000 | 0.000 | 0.000 | 0.000 | 0.000 | 0.001 | | | | | | | |
| **H** | 0.01 | 0.0316 | 0 | 0.04 | 79 | 0.000 | 0.000 | 0.000 | 0.000 | 0.000 | 0.000 | 0.000 | 0.033 | 0.209 | 0.99 | 0.02 | 0.61 | 0.07 |
| **I** | 0.1 | 0.0316 | 0 | 0.40 | 0.79 | 0.000 | 0.000 | 0.000 | 0.000 | 0.000 | 0.000 | 0.000 | 0.006 | 0.051 | 0.50 | 0.45 | 0.57 | 0.49 |

[a] indicated in the figures at the approximate location of $E_0/\hbar\omega$=1.4. [b] inverted region, dynamics at diabatic crossing energy; other approximations yield $\kappa_{LR}^{FD}$ =0.48, $\kappa_{LR}^{SD}$ = 0.28, and $\kappa_{LR}^{FD+SD}$ = 0.05.

$$H_{LR}^{CA}(Q)=\left\langle \phi_L^{CA}(r,Q_0)\middle|\mathbf{H}\middle|\phi_R^{CA}(r,Q_0)\right\rangle = J$$

$$H_{RL}^{CA}(Q)=\left\langle \phi_R^{CA}(r,Q_0)\middle|\mathbf{H}\middle|\phi_L^{CA}(r,Q_0)\right\rangle = J$$

and $J$ is the electronic coupling between the diabatic states, $r$ represents the electronic coordinate, $Q$ represents the chosen (antisymmetric) dimensionless nuclear coordinate, $Q_m$ is a displacement in this coordinate that locates the two harmonic potentials at different nuclear geometries, $\omega$ is the vibration frequency of the harmonic diabatic oscillators in the absence of coupling, and $E_0$ is an energy asymmetry that represents the energy (sometimes taken as a free-energy) change in a chemical reaction. Dimensionless nuclear coordinates are obtained by scaling say normal-mode coordinates by their zero-point displacement length[80] $\sqrt{\hbar/\omega}$. The diabatic wavefunctions have the same character at all values of the nuclear coordinate $Q$, and to emphasize Eqn. 1 specifies their evaluation at some specific coordinate $Q_0$. In Fig. 2, the main elements of the model are sketched.

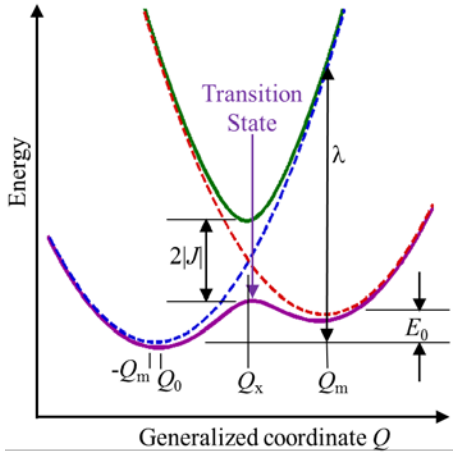


**Fig. 2**. The two-state diabatic model for general chemical reactions depicted by Eqns. (1) and (8): red, blue- harmonic diabatic surfaces $H_{LL}^{CA}(Q)$ and $H_{RR}^{CA}(Q)$, respectively; purple, green- $H_{--}^{BO}(Q)$ ground state and $H_{++}^{BO}(Q)$ excited BO adiabatic surfaces, respectively.

**b) Model parameters for different chemical systems.**

In Table 1, the chemical systems and model systems examined are categorized in terms of the three non-trivial variables $2|J|/\lambda$, $\hbar\omega/\Delta E$, and $E_0/\hbar\omega$ which specify the chemical scenario, relative vibrational to electronic energy scale, and relative asymmetry, respectively, where

$$\lambda = 2\hbar\omega Q_m^2 \tag{2}$$

is the reorganization energy and

$$\Delta E = (\lambda^2 + 4J^2)^{1/2} \tag{3}$$

indicates the overall energy scale. The reorganization energy is the energy difference between vertical and relaxed excitation of the diabatic states (see Fig. 2), whilst the adiabatic vertical excitation energies at the two minima of a double-welled ground state surface are approximately $\lambda \pm E_0$ provided that *either* $2|J|/\lambda \ll 1$ *or* $|E_0|/\lambda \ll 1$.[59] The values of the parameters used are taken from observed and calculated data,[3, 66, 68-79] as described elsewhere.[3, 59] Values for closed-shell systems are based on our renormalization scheme that maps these essentially multi-state problems onto an effective two-state model.[66] As this mapping is property dependent, we select parameters that relate to the key applications of each particular molecule.

**c) Full-quantum solution to the model using diabatic electronic basis states**

The vibronic eigenvalues $\varepsilon_j$ and eigenvectors $|\psi_j(r,Q)\rangle$ of **H** can readily be determined using standard methods[59] using the diabatic basis (Eqn. (1)), representing the eigenfunctions as

$$|\psi_j(r,Q)\rangle = \sum_{i=1}^{N} C_{ij}^{L} |\phi_L^{CA}(r,Q_0)\rangle |\chi_i^{L}(Q)\rangle + C_{ij}^{R} |\phi_R^{CA}(r,Q_0)\rangle |\chi_i^{R}(Q)\rangle \tag{4}$$

Here, $|\chi_i(Q)\rangle$ are harmonic-oscillator vibrational basis sets[80] centred at $Q$ = 0, truncated at $N$ functions per state. All matrix elements are evaluated analytically.[59] Calculations are mostly rapidly convergent and we use a typically grossly excessive value of $N$ = 256 functions.

**d) Full and approximate quantum solutions to the model using BO adiabatic electronic basis states**

Alternatively, application of the BO approximation[56, 81] to solve for the properties of **H** proceeds by diagonalizing it parametrically as a function of the nuclear coordinate $Q$ to yield the ground-state (-) and excited-state (+) potential-energy surfaces

$$\varepsilon_{\pm}(Q) = \frac{E_0}{2} + \frac{\lambda}{4} + \frac{\hbar\omega}{2}Q^2 \pm \left[\left(\frac{E_0}{2} - \hbar\omega Q_m Q\right)^2 + 4J^2\right]^{1/2} \tag{5}$$

and associated BO electronic wavefunctions

$$\begin{aligned} |\phi_-(r,Q)\rangle &= a(Q)|\phi_L^{CA}(r,Q_0)\rangle + b(Q)|\phi_R^{CA}(r,Q_0)\rangle \\ |\phi_+(r,Q)\rangle &= -b(Q)|\phi_L^{CA}(r,Q_0)\rangle + a(Q)|\phi_R^{CA}(r,Q_0)\rangle \end{aligned} \tag{6}$$

where the mixing coefficients are given by

$$a(Q) = \frac{J}{\left\{J^2 + \left[\varepsilon_- - \hbar\omega(Q+Q_m)^2/2\right]^2\right\}^{1/2}}, \quad \text{and} \tag{7}$$

$$b(Q) = \frac{\varepsilon_- - \hbar\omega(Q+Q_m)^2/2}{\left\{J^2 + \left[\varepsilon_- - \hbar\omega(Q+Q_m)^2/2\right]^2\right\}^{1/2}}.$$

However, using these BO wavefunctions as the basis describing the electronic motion, Eqn. (1) may be rewritten *without approximation*[56, 57] as $\mathbf{H}^{BO}(Q)$ where

$$\begin{aligned} H_{ab}^{BO}(Q) &= \langle \phi_a^{BO}(r,Q)|\mathbf{H}|\phi_b^{BO}(r,Q)\rangle \text{ for } a,b = +,- \text{ and} \\ H_{--}^{BO}(Q) &= \varepsilon_-(Q) + \Delta H^{DC}(Q) - \frac{\hbar\omega}{2}\frac{\partial^2}{\partial Q^2}, \\ H_{++}^{BO}(Q) &= \varepsilon_+(Q) + \Delta H^{DC}(Q) - \frac{\hbar\omega}{2}\frac{\partial^2}{\partial Q^2}, \\ H_{-+}^{BO}(Q) &= -H_{+-}^{BO}(Q) = \Delta P^{FD}(Q)\frac{\partial}{\partial Q} + \Delta H^{SD}(Q). \end{aligned} \tag{8}$$

Here,

$$\begin{aligned} \Delta H^{DC}(Q) &= \frac{\hbar^2\omega^2\lambda J^2}{4[2J^2 + \hbar\omega\lambda(Q-Q_x)^2]^2}, \\ \Delta P^{FD}(Q) &= \frac{-\hbar^2\omega^2\delta J}{2J^2 + \hbar\omega\lambda(Q-Q_x)^2}, \text{ and} \\ \Delta H^{SD}(Q) &= \frac{\hbar^3\omega^3\lambda J\delta(Q-Q_x)}{[2J^2 + \hbar\omega\lambda(Q-Q_x)^2]^2} \end{aligned} \tag{9}$$

provide the diagonal correction (DC) $\Delta H^{DC}$, first-derivative (nuclear momentum) correction (FD) $\Delta H^{FD} = \Delta P^{FD}(Q)\partial/\partial Q$, and second-derivative (nuclear kinetic energy) correction (SD) $\Delta H^{SD}$ to the BO approximation, with

$$Q_x = \frac{E_0}{\lambda}Q_m \tag{10}$$

being the nuclear coordinate at which the two CA states intersect.[59] An example BO surface for which the BO ground-state develops a transition state are shown in Fig. 2. Solving Eqn. (8) retaining all three correction terms provides a numerically exact solution to the original model Hamiltonian which we label as the full calculation (FC). The deduced

vibronic eigenvalues $\varepsilon_j$ plus all properties such as dipole moments, transition moments, etc., should therefore be the same as those determined using the diabatic basis directly from Eqn. (1). However, it is also possible to generate a range of approximate solutions depending on which of the coupling terms from Eqn. (8) are retained. The BO approximation corresponds to neglecting all three corrections whilst the BH approximation retains only DC, ignoring the FD and SD surface hopping contributions. We also consider approximations in which just FD or SD are included, etc..

Numerical solution of Eqn. (8) proceeds similarly to that of Eqn. (1), using again a vibrational basis set of $N$ harmonic-oscillator vibrational basis wavefunctions $\left|\chi_i(Q)\right\rangle$ centred at $Q$ = 0, writing the eigenfunctions as $\left|\psi_j(r,Q)\right\rangle$

$$= \sum_{i=1}^{N} C_{ij}^{-} \left|\phi_{-}(r,Q)\right\rangle \left|\chi_i^{-}(Q)\right\rangle + C_{ij}^{+} \left|\phi_{+}(r,Q)\right\rangle \left|\chi_i^{+}(Q)\right\rangle \qquad (11)$$

Whilst solution to Eqn. (1) is rapid and efficient, for Eqn. (8) scenarios involving small cusp diameters lead to extremely large basis-set requirements for the evaluation of BO breakdown and we report results that are either converged or nearly so using at $N$ = 1024 functions.[59] Required matrix elements are evaluated numerically.[59, 80]

**e. Determining the entanglement.**

The primary observable consequences of entanglement in quantum systems stem from the results of making measurements for one of the observable properties of the system.[1] If entanglement is present then such measurements also reveal unexpected information concerning other aspects of the system. Therefore the nature of the measurement must always be specified when considering entanglement. Measurement projects a quantum wavefunction onto some basis, and calculations of this entanglement must mimic this. This computational aspect is unusual as most observable properties arise independent of the basis in which the calculations are performed. While unitary transformations of basis sets do not modify entanglement,[1] Eqn. (7) is non-unitary owing to its parametric dependence on the nuclear coordinate. Hence the entanglement measured in the diabatic basis CA will be *different* to that measured in the BO basis using FC, whereas other properties such as energies and dipole moments are *independent* of the choice of the electronic basis.

For not just eigenstates but for any general time-dependent wavefunction expressed in one of these forms, the entanglement is calculated by first determining the appropriate reduced electronic density for wavefunction $j$[1, 3]

$$\boldsymbol{\rho}_j = \begin{bmatrix} \rho_j^{--} & \rho_j^{-+} \\ \rho_j^{-+} & \rho_j^{++} \end{bmatrix} \text{ or } \boldsymbol{\rho}_j^{CA} = \begin{bmatrix} \rho_j^{LL} & \rho_j^{LR} \\ \rho_j^{LR} & \rho_j^{RR} \end{bmatrix}, \qquad (12)$$

where

$$\rho_j^{ab} = \sum_{i=1}^{N} C_{ij}^{a} C_{ij}^{b} \ , \qquad (13)$$

where either $a,b \in \{+,-\}$ or $a,b \in \{\mathrm{L},\mathrm{R}\}$. In terms the von Neumann entropy, the entanglement is then given by[1]

$$S_j = -\mathrm{Tr}(\boldsymbol{\rho}_j \log_2 \boldsymbol{\rho}_j) \text{ or } S_j^{CA} = -\mathrm{Tr}(\boldsymbol{\rho}_j^{CA} \log_2 \boldsymbol{\rho}_j^{CA}) \, . \qquad (14)$$

Note that it is also possible to obtain this entanglement equivalently by an analogous procedure utilizing instead the reduced vibrational density.[3] The von Neumann entropy is widely accepted as the best measure of quantum entanglement for pure quantum states defined on bipartite systems, such as that considered here. This is because it satisfies many desired criteria including: vanishing for separable states, monotonicity (it does not increase under local operations or classical communication between the subsystems), additivity, convexity, and continuity.[82]

The entanglement developed as a function of time during the motion of wavepackets is obtained by expressing the initial wavepacket as a Gaussian distribution of nuclear position probability on a BO surface as say

$$\left|\Psi(r,Q;0)\right\rangle = \sum_i \left\langle \chi_i^{-}(Q) \,|\, \pi^{-1/4} \exp\left[-(Q-Q_I)^2/2\right] \right\rangle \left|\phi_{-}^{BO}(r,Q)\right\rangle \left|\chi_i^{-}(Q)\right\rangle \qquad (15)$$

where $Q_I$ is the initial location of the centre of the wavepacket. This is then projected onto the 2$N$ vibronic eigenstates of the BO electronic Hamiltonian (Eqn. (8)) as

$$\left|\Psi(r,Q;t)\right\rangle = \sum_{j=1}^{2N} d_j(t) \left|\psi_j(r,Q)\right\rangle . \qquad (16)$$

It's quantum dynamics is evaluated analytically using

$$d_j(t) = d_j(0) \exp\left(-i\varepsilon_j t/\hbar\right) . \qquad (17)$$

The wavefunction is then rewritten into the form of Eqn. (11) (or Eqn. (10)) and the entanglement determined.

## 3. Results

**a. Entanglement in the ground-vibronic state, first-excited vibronic state, and transition-state adiabatic wavefunctions**

The energy of the ground-vibronic wavefunction is important in determining e.g. heats of reaction, while this and the energy of the next-lowest vibronic level determine the lowest spectroscopic transition energy; other properties of these wavefunctions determine transition moments, Stark susceptibilities, etc.. Here we use entanglement to quantify how quantum in nature these eigenfunctions appear within the BO approximation, a result that pertains to the suitability of using just a single adiabatic electronic state to describe system properties.

Alternative commonly used measures for intrinsic quantum nature include the values of the excited-state density $\rho^{++}$ and the off-diagonal density-matrix element $\rho^{-+}$ themselves, and we compare these measures with the associated entanglement in Fig. 3 and Table 1 for three eigenfunctions of the two-state one-mode model. These eigenfunctions are: the lowest vibronic energy level (0), the first vibronic excited-state (1), and the eigenstate closest in energy to that of the transition state, when one exists. The ground-state BO surface has no transition state whenever[59]

$$\left(\frac{\hbar\omega}{\Delta E}\right)^2 \left(\frac{E_0}{\hbar\omega}\right)^2 \geq \left[1 - \left(\frac{2|J|}{\lambda}\right)^{2/3}\right]^3 \left[1 + \left(\frac{2J}{\lambda}\right)^2\right] . \qquad (18)$$

These regions are indicated by dark-grey shading in the figure.

If classical molecular dynamics on the ground-state adiabatic surface is to be reliable, then all three measures of the wavefunction $\rho^{++}$, $\rho^{-+}$, and $S$ need to be very small whereas all three measures approach unity in the worst-possible cases. Fig. 3 shows that the individual density components $\rho^{++}$ and $\rho^{-+}$ sometimes have similar qualitative dependencies on the model parameters $2|J|/\lambda$ , $\hbar\omega/\Delta E$ , and $E_0/\hbar\omega$ whereas sometimes they behave quite differently. The entanglement,

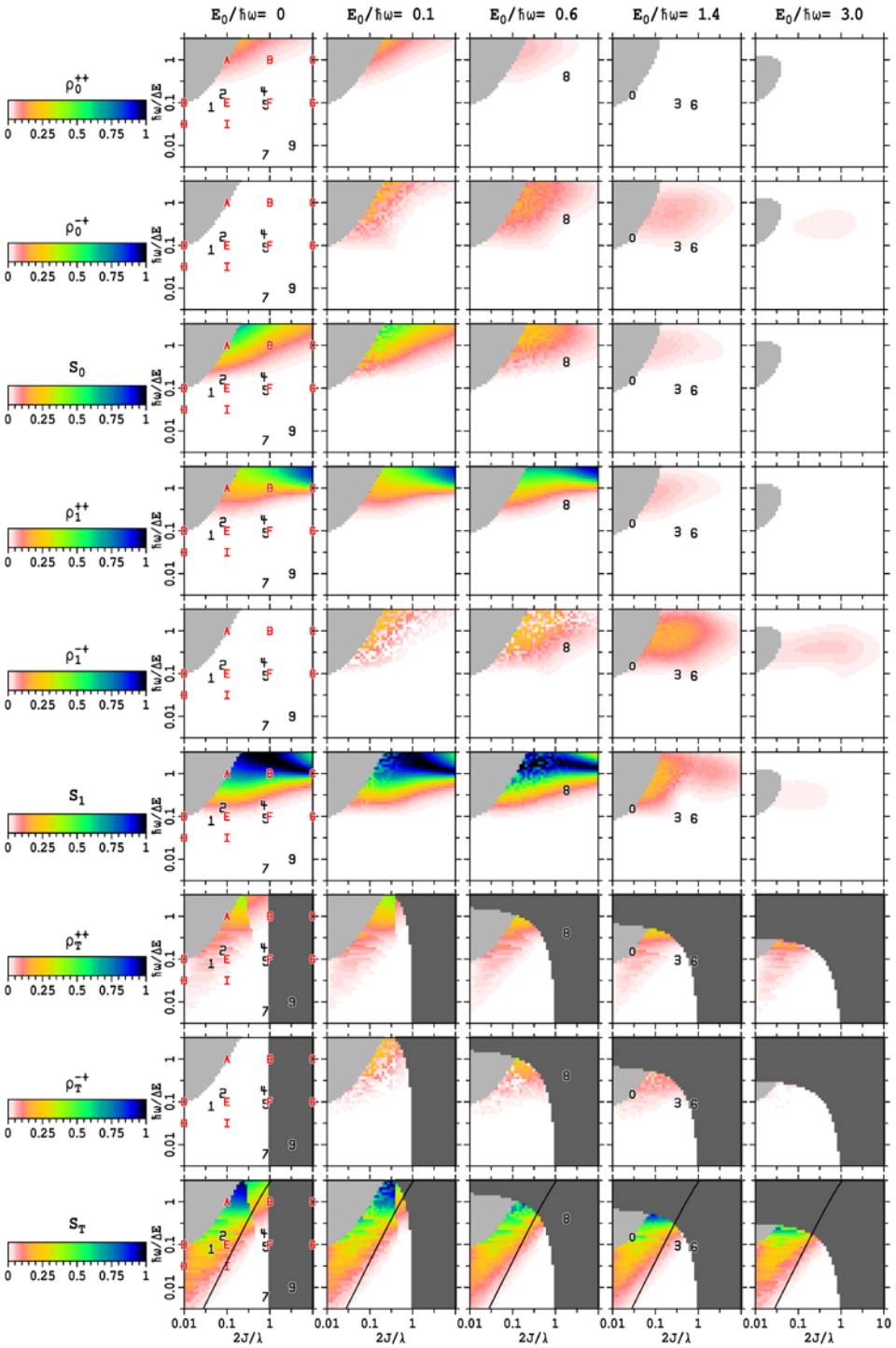


**Fig. 3** Measures of BO wavefunction mixing for the lowest (0) , first-excited (1), and near transition-state (T) vibronic eigenfunctions of the two-state one-mode model: $\rho^{-+}$ - electronic off-diagonal density, $\rho^{++}$ - electronic excited-state density, *S* - entanglement. Model compounds **1**-**9** and points **A**-**I** are indicated; regions with poor numerical convergence are shown in light grey whilst those without a transition state are in dark grey. The dashed line is for $Q_c=8^{1/2}$, indicating where $\Delta\Delta E^{+}=\hbar\omega$ .

which from Eqn. (14) is sensitive to both density components, indicates that classical mechanics would be unsuitable whether or not this feature can be attributed to $\rho^{++}$ and/or $\rho^{-+}$. It therefore provides a general way for the interpretation of complex data, the entanglement being only a single number independent of the level of complexity in the density matrix.

Fig. 3 shows that the entanglement in the ground-state vibronic eigenfunction is small for all of the sample molecules **0** – **9**. This is expected as molecules like ammonia, benzene, etc. are known to be accurately described using the BO approximation. However, it is conceivable that even small levels of entanglement could be significant, suggesting that deviations from BO results could be detectable In particular, for the iconic molecule **4** (BNB), *S*=0.01, while for the technologically relevant

systems **2** (Alq3) $S$=0.02 and for **8** (PRC) $S$=0.02. Significant entanglement is predicted only for systems with $\hbar\omega / \Delta E > 0.5$. In this region Jahn-Teller effect must be included before conclusions can be drawn, however.

BO entanglement within the first excited vibronic level is generally larger than that in the ground vibronic level as greater mixing occurs at higher energies. From Table 1, the largest entanglement calculated for any of the model compounds is 0.11 for **8** (PRC), with entanglement also becoming noticeable also for **1** (DPP), **3** ($^3$PYR), and **5** CT. The entanglements within wavefunctions at energies corresponding to the transition state become quite large for the weakly coupled electron-transfer molecules **1** (DPP) and **2** (Alq3), reaching 0.23 and 0.34, respectively. As the electronic coupling becomes weaker, the entanglement increases indicating enhanced failure of the BO approximation. This is no surprise as non-adiabatic computational methods are almost always used to study such processes; rather it is surprising just how little entanglement is actually developed for quite small values of $2|J|/\lambda$ of order 0.04 – 0.08, and that entanglement decreases significantly as the vibration frequency falls. Reduced vibration frequencies would occur e.g. if an electron transfer process was most strongly coupled to low-frequency solvent modes rather than to intramolecular vibrations.

The three BO correction terms in Eqn. (9) can all be expressed simply[59] in terms of the cusp diameter

$$Q_c = \frac{2|J|}{\lambda} Q_m \approx 0.16 \left( \frac{2|J|}{\lambda} \right)^{3/4} \left( \frac{\hbar\omega}{\Delta E} \right)^{-1/2} . \qquad (19)$$

The smaller the value of this diameter, the more profound the effects of BO breakdown are. For example, the DC term takes on a maximum value at $Q$=$Q_{\rm m}$ of

$$\Delta\Delta E^{\dagger} = \frac{\hbar\omega}{8Q_c^2} = \frac{(\hbar\omega)^2 \lambda}{16 J^2} = \frac{\hbar\omega}{4} \left( \frac{\hbar\omega}{\lambda} \right) \left( \frac{2J}{\lambda} \right)^{-2} \qquad (20)$$

and can be thought of as providing a sharp spike in the potential close to the transition state of width $Q_c$. When $Q_c = 8^{-1/2} \sim 0.35$, $\Delta\Delta E^{\dagger} = \hbar\omega$ and so processes at the transition state must be affected. The locus of this line is shown on Fig. 3 and roughly correlates with the onset of entanglement in the wavefunctions at the transition state. At lower energies than the transition state of non-Jahn-Teller systems, the effect of the spike is rapidly diminished and so the entanglement falls off.

In summary, to have significantly entangled adiabatic wavefunctions at the transition state, i.e., significant failure of the Born-Oppenheimer approximation, the energy gap there needs to be small compared to that at the relaxed geometry ( $2|J|/\lambda$ small, deep cuspy double well) and the vibration frequency has to be significant compared to the electronic energies ( $\hbar\omega / \Delta E$ not small). This is in accordance with traditional qualitative understandings of BO breakdown but here is presented quantified using a simple model chemical system that shows how ground-vibronic-level properties relate.

**b. Entanglement in the ground-state and transition-state diabatic wavefunctions: implications for quantum qubits**

As conceived experiments could make measurements in a spatially localized basis that closely resembles the diabatic states L and R, entanglement in this basis is of fundamental interest for quantum information applications. Previously[3] we have mapped out this entanglement for the ground-state vibronic wavefunction and shown that it correlates poorly with the diabatic-state densities but is closely related to whether or not the vibrational density profile of the ground vibronic level is bimodal (i.e., has two local maxima at different geometries and an intermediary local minimum). In Fig. 4 some of these critical results are reproduced where they are compared to the off-diagonal density profile $\rho_0^{LR}$ and extended to describe the vibronic wavefunction closest in energy to the transition state.

Concerning the ground-state wavefunction, the new results indicate that while the entanglement appears to correlate with the off-diagonal density for symmetric systems with $E_0$ = 0, no general correlation is found. Hence, the entanglement provides a different perspective on the system properties than is obtained using conventional representations of the density. The bimodality of the density may be assessed as done previously[3] using the exact wavefunction but in addition it is possible to use the BO approximation to calculate it, with the two approaches compared in Fig. 3. Good agreement is generally obtained, indicating that BO calculations can provide significant physical insight into this measureable entanglement property; they overestimate bimodality for small values of $2|J|/\lambda$. However, as in this region the local minimum in the BO density profile is very shallow and is removed by the addition of a small amount of excited-state character into the wavefunction. Bimodality of the density is a property of general interest, related to technologically relevant quantum phase transitions.[83]

The results shown in Fig. 4 for the density and entanglement of the vibronic level closest in energy to the BO transition state has a striated nature owing to the changing nature of this level with the system parameters. However, it is clear that the entanglement near the transition state is in general much larger than that found for the lowest vibronic level, as one would expect. Also, the entanglement in the lowest vibronic level is large only for $E_0$ = 0 and is very fragile,[3] often decreasing dramatically for very small asymmetries $E_0 / \hbar\omega \sim$ 0.01, whereas the entanglement at the transition state is robust, decreasing slowly with increasing asymmetry. Interestingly, this entanglement seems to be maximal near the line $Q_c = 8^{-1/2} \sim 0.35$ shown on Fig. 4 for which $\Delta\Delta E^{\dagger} = \hbar\omega$. While we have argued that the fragility of the ground-level entanglement would effectively prevent the construction of robust chemical qubits,[3] qubit operation based on much higher energy levels would in principle be possible.

Ammonia **7** is of particular note as methods have been conceived that utilized it as a qubit in a chemical quantum information device.[4] It does have a bimodal density profile with well characterized vibrational energy levels in each well and with an observed tunneling process which, as Fig. 3 shows, develops large entanglement $S_0^{CA} \sim$1. This entanglement disappears at $E_0 / \hbar\omega$ = 0.01, however, indicating that it is very fragile and extremely sensitive to environment. While methods have been conceived for minimizing environmental interactions in chemical qubits,[4-9] the extreme sensitivity of the lowest-energy level to environment does not indicate a promising scenario. However, with only a few additional quanta of torsional vibration, ammonia can be excited to energy levels spanning the transition state for which the entanglement is insensitive to environment. Maintaining coherence at such higher energies is of course intrinsically more difficult, but the changing nature of the wavefunctions with energy may reduce coherence demands to facilitate a practical device. Of all the molecular systems considered, those with the most robust entanglement suitable for use in qubits are **1** DPP and **2** Alq3.

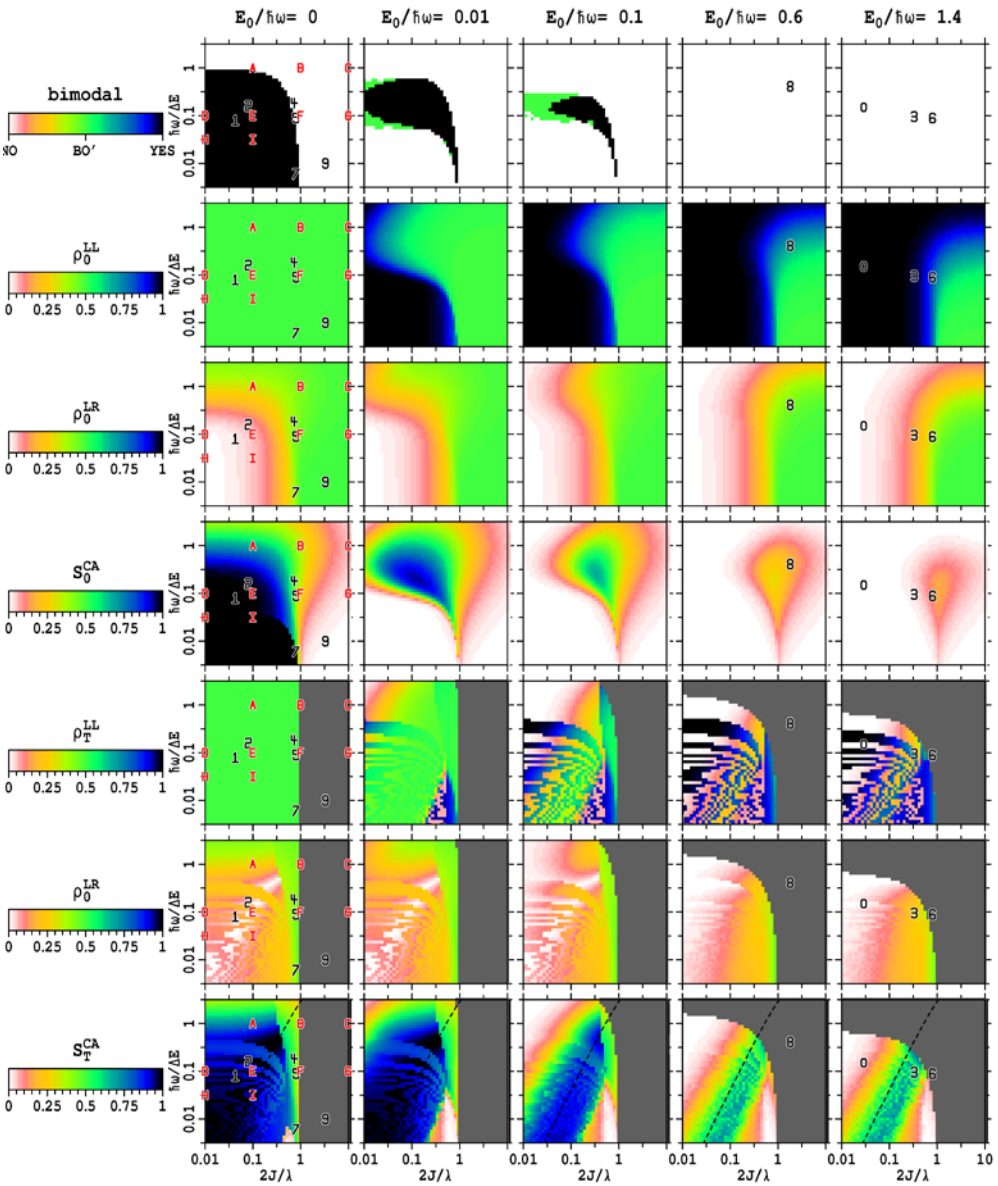


**Fig. 4** Measures of diabatic (CA) wavefunction mixing for the lowest (0) and near transition-state (T) vibronic eigenfunctions of the two-state one-mode model: $\rho^{LR}$ - electronic off-diagonal density, $\rho^{LL}$ - diabatic state density, $S$ - entanglement. Model compounds **1**-**9** and points **A**-**I** are indicated, see Table 1; regions without a transition state are shown in dark grey. The dashed lines indicate where $Q_c = 8^{-1/2}$, making the diagonal correction to the transition-state energy equal to the vibrational spacing.

### c. Entanglement between vibrations and adiabatic states developed during chemical reactions

In Figs. 3 and 4, the properties of the closest eigenstate to the transition state were considered. However, few experiments proceed utilizing such eigenstates as chemical dynamics usually involves a non-stationary initial state that converts into a product state when it decoheres. A useful model for general processes of this type is the dynamics of an initial coherent-state wavepacket. Such wavepackets move coherently (i.e., their centres evolve according to classical mechanics and they do not change shape) in the absence of coupling, $J$=0. When coupling is included, the wavepacket will fracture into different components on encountering the transition state (or diabatic surface intersection point for non-classical reactions for which Eqn. (18) indicates no transition state). One component will pass the transition state on the ground-state surface, either because it has enough energy or else because it tunnels through. Another component will be bounced directly back, mostly because its energy does not exceed the barrier of the BH potential (the BO transition-state energy + $\Delta\Delta E^{\dagger}$). The third component gets transferred to the excited state surface. By selecting an ensemble of wavepackets that mimics the state of (thermally or photochemically) prepared initial reactants, rates of chemical reactions can be determined. Fig. 5 shows how each *single* wavepacket is scattered using calculations based on the BO approximation, monitoring the entanglement that develops between the vibrational motion and BO electronic states when the cusp region near the transition state is encountered.

Ten sample trajectories are considered, examining the 4 parameter values **D**, **E**, **H**, and **I** as well as molecule **0** ($FcPC_{60}$) and **5** (CT). These trajectories are run at either the energy of the transition state (top frames of Fig. 5), pertinent to thermal reactions over a transition-state barrier, or at four times this

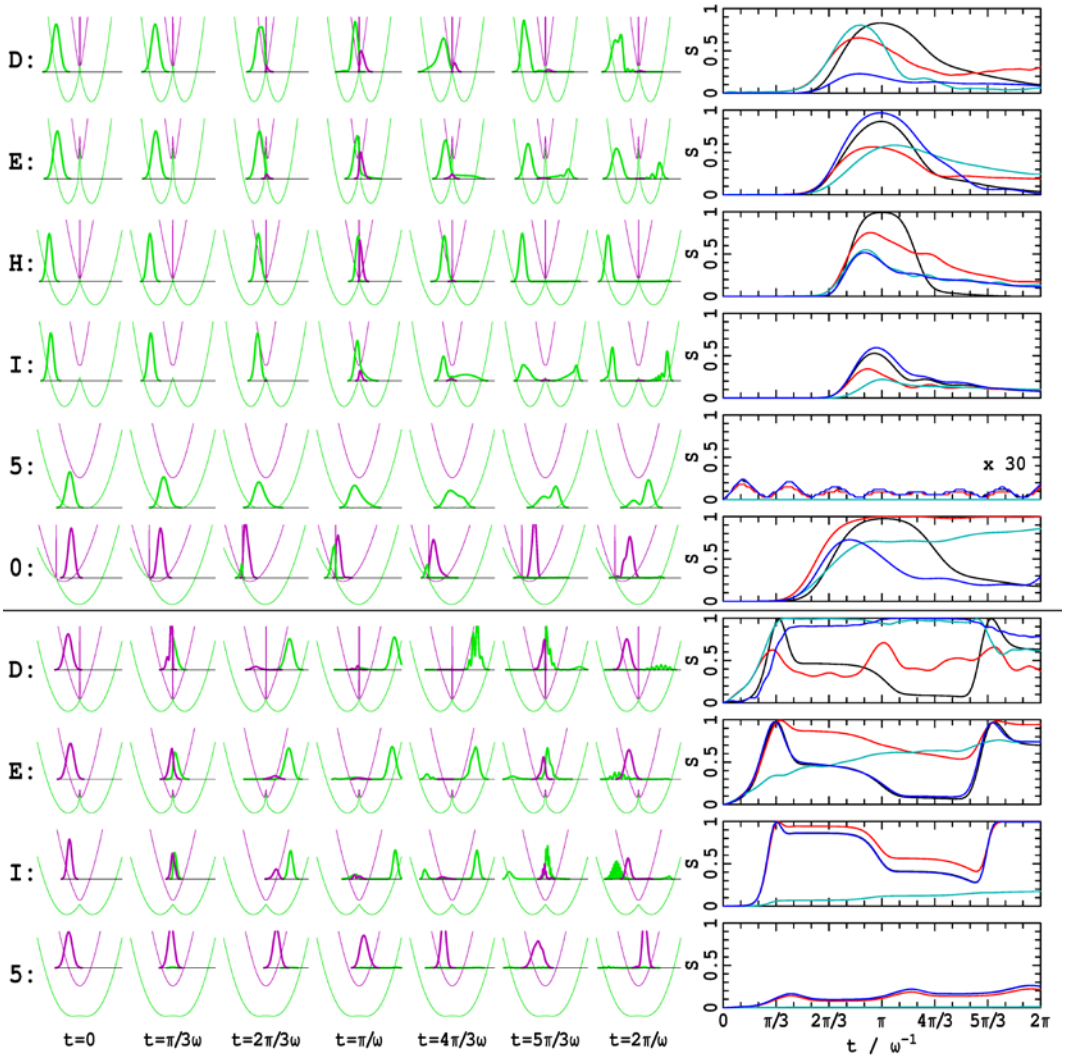


**Fig. 5** Quantum dynamics of a Gaussian wavepacket starting at either the energy of the transition state (upper frames, pertinent to thermal reactions) or four-times the energy of the diabatic crossover (lower frames, pertinent to photochemical processes) for characteristic points **A**, **E**, **H**, and **I** (see Table 1) as well as for molecules **0** ($FcPC_{60}$) at **5** (CT). The left frames show the BH adiabatic potential-energy surfaces (green- ground state, purple- excited state) and the wavepacket's vibrational density resolved onto these states, while the right frames show the development of the entanglement in the BO basis using: black- exact dynamics FC, red- DS-only approximation, blue- FD-only approximation, and cyan- FD+SD approximation.

energy for **D**, **E**, and **I** or at the value of the reorganization energy for **5** (bottom frames), pertinent to high-energy photochemical processes. While the low-energy trajectories should provide good qualitative descriptions of the properties of all model chemical systems considered, the high-energy trajectories depict *only part* of the story as these reactions could actually proceed over conical intersections and hence require at least two nuclear coordinates to properly describe.

All trajectories start on one of the BO adiabatic potential-energy surfaces. It is perhaps simpler and more intuitive to depict the initial conditions in terms of diabatic surfaces instead, but for all cases considered the starting points are in a region in which one diabatic surfaces does indeed dominate the adiabatic one. Our approach is chosen here so as to focus on the effects of the BO approximation. The dynamics is followed for one period of the coherent motion that would be produced if $J$=0. After this time, a fraction $\kappa_{LR}$ of the wavepacket gets transferred to the other diabatic state. We assume that the decoherence processes that would trap the products act infinitely quickly and hence ignore any subsequent dynamics, dynamics that would in reality be controlled by interference effects and be very sensitive to the number of vibrational modes considered in the analysis. However, this is a useful approximation that is central to the Landau-Zener[84, 85] and other models of chemical reaction kinetics.[62] Table 1 shows this fraction for all of the sample molecules and data points that support transition states, evaluated using the BO approximation, the BH approximation, and the full calculation (FC) embodying all three BO-breakdown corrections. In the region of the parameter space for which the BO approximation works well (e.g., for **7** $NH_3$), all three methods predict similar reaction yields, but otherwise large differences appear, especially for **1** DPP and **2** Alq3.

Fig. 5 shows the time evolution of the wavepacket's vibrational density, projected onto either the BO ground state (in green) or excited state (in purple). In addition, the BH adiabatic potential-energy surfaces are also shown. These surfaces differ from the more usual BO ones $\varepsilon_{\pm}(Q)$ in that the correction term $\Delta H^{DC}(Q)$ is also added. This correction adds a sharp spike of diameter $Q_c$ and height $\Delta\Delta E^{\dagger} = \hbar\omega / 8Q_c^2$ (Eqn. (20)) near the

**Table 2.** Summary of the BO correction terms that must be included in the Hamiltonian in order to model realistically reaction rates, energetics, spectroscopy, or the entanglement in the BO basis.

| Systems | Energy[a] | $Q_c$ | Reaction rate described by | Entanglement described by |
|---|---|---|---|---|
| **A** | low | 0.07 | [needs $N > 1024$ basis functions] | |
| **1**,**2**,**B**,**D**,**E**,**H** | low | <0.6 | [c] | BO+DC+FD+SD |
| **3**,**4**,**5**,**8**,**I** | low | 0.6-1.7 | [c] | BO+FD+SD |
| **6**,**7**,**9**,**C**,**F**,**G** | low | >1.6 | [c] | BO+FD |
| **D** | med. | 0.02 | BO+DC | BO+DC+FD+SD |
| **E** | med. | 0.22 | BO+DC+FD+SD | BO+DC+FD+SD |
| **H** | med. | 0.04 | BO+DC+FD+SD | BO+DC+FD+SD |
| **I** | med. | 0.40 | BO+DC | BO+FD+SD |
| **5** | med. | 1.68 | BO | BO+FD |
| **0** | med.[b] | 0.06 | BO+DC+FD+SD | BO+DC+FD+SD |
| **D** | high | 0.02 | BO+DC+FD+SD | BO+DC+FD+SD |
| **E** | high | 0.22 | BO+FD+SD | BO+FD+SD |
| **I** | high | 0.40 | BO+FD | BO+FD+SD |
| **5** | high | 1.68 | BO+FD | BO+FD |

[a] low- the lowest-energy spectroscopic transition, med.- thermal reactions at the transition-state energy, high- photochemical reactions with significant excess energy. [b] inverted region. [c] lowest-level energies and spectroscopy require: BO only for **3**,**7**,**9**,**G**,**H**,**I** with $\hbar\omega / \Delta E < 0.1$, BO+DC for **0**,**1**,**2**,**4**,**5**,**6**,**D**,**E**,**F** with $0.08 < \hbar\omega / \Delta E < 0.18$, and BO+DC+FD+SD for **8**,**B**,**C**with $\hbar\omega / \Delta E > 0.6$.

transition state,[59] see Table 1.

Fig. 5 also shows the entanglement between the BO electronic states and the vibrations that develops during the trajectories. Not only is the actual entanglement shown stemming from the full calculation FC utilizing all 3 BO-breakdown corrections but also the entanglement stemming from three approximate calculations: inclusion of only the FD correction, as is commonly applied in most calculations of BO breakdown, inclusion of only the SD correction, and inclusion of FD+SD only. The BO and BH approximations themselves are adiabatic and hence generate no entanglement; the entanglements from the full calculations at the critical time of $t = \pi / \omega$ are shown in Table 1.

Table 2 presents a qualitative summary of the effects seen in Fig. 5, indicating the minimum number of BO correction terms that must be included in order to obtain reasonable predictions of entanglement for the depicted chemical scenarios. These results are combined with those for the entanglement of the low-energy eigenfunctions discussed earlier. They are also compared to previously obtained[59] qualitative conclusions concerning the importance of the three BO breakdown corrections deduced by examining calculated spectroscopic properties and reaction rates. In this table, properties of ground-vibronic-level wavefunctions are labelled *low*-energy ones, thermal reaction rates over a transition state are labelled *medium*-energy properties, whilst rates for photochemical processes with significant excess energy are labelled *high*-energy properties.

Run at the transition-state energy (medium energy), the trajectory for sample point **D** ( $2J / \lambda = 0.01$, $\hbar\omega / \Delta E = 0.1$, $E_0 = 0$) shown in Fig. 5 depicts a classic weakly coupled symmetric electron-transfer reaction in the "non-adiabatic" regime. The initial wavepacket moves coherently until it strikes the transition-state region at which it is mostly reflected by the large BH transition-state energy spike of height $\Delta\Delta E^{\dagger} = 250\,\hbar\omega$ (Table 1), but a small component does undergo surface hopping to the BO excited state induced by the FD and SD terms. The fraction that surface hops quickly hops back, however, and becomes reunited with the directly reflected wavepacket. Using just $N$=1024 basis functions per state is slightly inadequate for this trajectory, however, as by $t = 2\pi / \omega$ a near complete reformation of the original wavepacket is actually expected (see the converged propagation in the CA basis shown later in Fig. 6) whereas the displayed function is slightly distorted. Table 1 shows that the BH approximation correctly predict that just 2% of the wavepacket reacts during this process and hence the reaction perhaps should not be described as "non-adiabatic", instead it appears to be just "non-Born-Oppenheimer". Indeed, in Table 2 this reaction is depicted as being well described using the BH (i.e., BO+DC) approximation. However, Fig. 5 shows that the entanglement becomes very large amidst the encounter with the transition state, reaching $S = 0.81$ at $t = \pi / \omega$. The BH adiabatic approximation completely misses this entanglement and so whilst some properties of the system may be well described using an adiabatic method, this is not a general result. Table 2 indicates that all BO breakdown corrections (DC+FD+SD) must be included in order to adequately calculate the entanglement for this system as all approximate methods that include surface hopping in some form but neglect the DC correction lead to relatively poor descriptions of the entanglement.

Trajectory **E** is a variant of this trajectory for which the coupling is increased an order of magnitude to $2J / \lambda = 0.1$. Now $\Delta\Delta E^{\dagger}$ is just $2.5\,\hbar\omega$ and so the DC correction no longer acts to reflect the incoming wavepacket. The product yield increases to 24% but now all correction terms must be used for the calculation of both the yield and the entanglement (Table 2). Interestingly, the entanglement profiles are somewhat insensitive to the change in the coupling. Trajectory **H** also involves a much reduced BH barrier correction of $\Delta\Delta E^{\dagger} = 79\,\hbar\omega$ so that direct reflection is also reduced, arising here through reduction of the vibration frequency to $\hbar\omega / \Delta E$ =0.0316. While the reaction yield remains at just 2% owing to the increased effects of surface hopping, the entanglement profiles look qualitatively similar. To complete this series, trajectory **I** evokes both changes simultaneously to make the BH barrier insignificant and also induce a band gap between the BO (and BH) surfaces). Now the BO approximation provides a useful description of the dynamics but the DC correction should still be included. The manifested entanglement is reduced by nearly half and is adequately modeled using only the surface-hopping FD+SD. In addition we also show dynamics for **5** (CT), a strongly coupled system showing a very shallow double well that the bimodality plot in Fig. 4 reveals does not support zero-point vibration. The BO approximation works well for this molecule, with any deviations, including the buildup of a small amount of entanglement that can be adequately described using the FD correction alone.

Also shown in Fig. 5 is the dynamics of a wavepacket mimicking photochemical charge recombination in **0** ($FcPC_{60}$), a medium-energy reaction that occurs in the Marcus inverted region where there is no transition state. While the three BO-breakdown corrections act in qualitatively different manners in the normal and inverted regions,[59, 86] the effect of the BH correction is still to block reaction while the entanglement profiles look qualitatively similar. The major qualitative difference between reactions in the inverted region and those in the normal region is that entanglement is essential only for reactions in the inverted region, but this feature is not reflected in the entanglement profiles themselves.

Finally, Fig. 5 shows trajectories for scenarios **D**, **E**, and **I** run at high energy as would be appropriate for many photochemical reactions. The BH barrier still reflects the incoming wavepacket when it is high enough, but the effect is much less than that for thermal trajectories owing to the presence of the excess wavepacket energy. Even for scenario **D** for which $\Delta\Delta E^{\dagger} = 250$

$\hbar\omega$ and the excess energy above the BO transition state is only 7.3 $\hbar\omega$, the amount of reflection remains modest. This indicates that surface hopping *before* the barrier is accessed and/or tunnelling *through* the barrier remains significant throughout a large region of the parameter space when the reactant velocity is high. Like reactions in the inverted region, these photochemical reactions only occur via surface hopping and so only occur when there is entanglement and so from a kinetics perspective they behave fundamentally differently[59, 86] to medium-energy thermal reactions, as is clear from Table 2. The behaviour of the entanglement is analogous to that found for thermal trajectories that do not critically require entanglement, however, becoming large only when the wavepacket encounters the transition state and being attenuated only by the buildup of a significant band gap between the adiabatic states.

Table 2 indicates that the BO entanglement manifested in low-energy eigenfunctions and in reactive trajectories follows a simple pattern controlled by the value of the cusp diameter. When $Q_C$ > 1.6, use of only the FD correction is sufficient to model it whereas for $Q_C$ < 0.2-0.6 all 3 corrections are required, with just the two surface-hopping corrections FD+SD sufficing in the intermediary region. This picture conforms to basic expectations of the effects of BO breakdown based on the known relationships linking the 3 correction terms: DC is the square of the FD terms whilst SD is its derivative.[59-62] This simplicity is lost when complex observed phenomena are considered, however. Table 2 shows that the lowest spectroscopic transition energy scales not with the cusp diameter but rather with the vibrational to electronic energy ratio $\hbar\omega / \Delta E$. It also shows that chemical reaction rates scale in this expected fashion only for high-energy photochemical reactions for which the DC correction acts in a specific but unimportant way, whereas for medium-energy thermal reactions, DC plays the critical role. Indeed, for large cusp diameters great than 1, the BO approximation itself is adequate to describe kinetics, adding the DC correction is required for slightly smaller values, values of order 0.04 < $Q_C$ < 0.2 need the full calculation including all correction terms DC+FD+SD, yet even smaller values require just using DC.

### d. Entanglement between vibrations and diabatic states developed during chemical reactions

In Fig. 6 is shown the same dynamics as in Fig. 5 but this time the wavepacket is shown projected onto the diabatic electronic states and the entanglement is that as manifest in the CA basis. This dynamics comes from the direct use of Eqn. (1) rather than through the introduction of the BO approximation.

For thermal trajectories at the transition-state energy, essentially coherent dynamics of the initial diabatic wavepacket is obtained for the weakly coupled electron-transfer-type system **D**, with diabatic surface hopping increasing (i.e., the BO approximation becomes more apt) as the cusp diameter increases through systems **E**, **H**, **I**, and **5**. The (in principle measureable) entanglement in the diabatic basis increases accordingly, becoming large for cases **E**, **I**, and **5**. Unlike entanglement in the BO basis, this entanglement remains after the wavepacket leaves the transition-state region. Reactions in the inverted region generate little entanglement, and high-energy photochemical reactions have properties analogous to the associated thermal ones. Note that the repetitive encounters of the wavepacket with the transition state followed for the low-reaction-rate high-energy collisions simply increase the entanglement. In the CA basis all reactions require entanglement to proceed but these calculations suggest that the rate of production of this entanglement does correlate in some way with the rate constant for the reaction between the reactant and product diabatic surfaces.

## 4. Conclusions

Using a simple model representing many chemical kinetic and spectroscopic properties, we have looked at the entanglement that develops between adiabatic electronic states and the vibrational motion as well as that which develops between diabatic electronic states and the vibrational motion. These are done both for the lowest energy eigenstates of the system and for eigenstates near the energy of the transition state, as well as for the dynamics of wavepackets undergoing chemical reactions at the energy of the transition state or well above. Sometimes the processes considered behave such that they could be adequately modeled using classical adiabatic force fields and sometimes they instead appear to be highly quantum in nature. As entanglement is now often regarded as being the quintessential descriptor of quantum effects[1] we investigate the correlation between the two sets of phenomena. This is done bearing in mind more traditional descriptors of the quantum nature of a system, the nature of the associated diagonal and off-diagonal elements of the density matrix. Does entanglement tell us different information than comes from the traditional descriptors? Does the entanglement tell us anything about how to calculate key experimentally measured properties such as reaction yields?

No general answers to these basic questions emerge as findings are context sensitive. For single eigenfunctions of either low energy or the energy of the transition state, the entanglement tells little new information concerning BO breakdown beyond what is apparent from consideration of more traditional density-matrix descriptors. For reactive trajectories performed using BO methods, the entanglement becomes large whenever the transition-state region is encountered and the BO approximation fails, as one would expect. However, the amount of effort required to accurately calculate this entanglement scales in a very simple way with the diameter of the cusp induced by the BO approximation. For small cusp diameter, only the leading term in the expansion of the exact Hamiltonian in terms of BO states, the FD term, is important. As the diameter decreases and BO breakdown becomes more profound, first the SD term must additionally be included and then finally the DC term. This orderly progressive failure of the BO approximation is not reflected in the calculation of other properties such as chemical reaction rates for which each individual term gains special significance depending on the nature of the specific rate process being considered.[59] Indeed, orderly failure is in general not expected for mathematical systems with cusps according to general considerations of the Catastrophe theory.[87-90] Thus entanglement does tell us important information concerning the structure of BO breakdown but conversely it cannot be used to determine how to calculate general system properties. However, it provides an easy to calculate measure of the quality of a wavefunction that is different to the energy-based criteria often used to judge wavefunction convergence, a measure that may relate more to the requirements of other wavefunction properties such as transition and dipole moments.

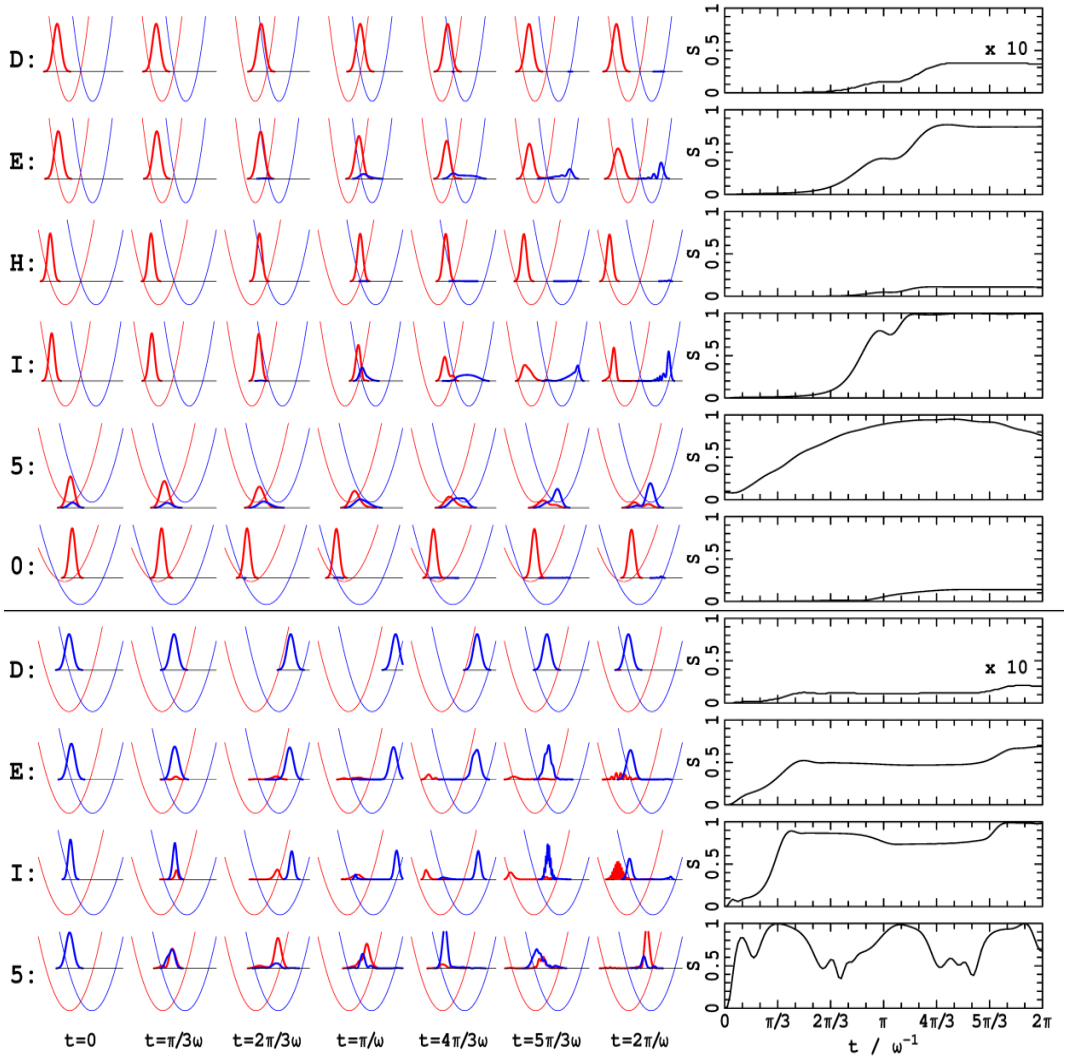


**Fig. 6** Quantum dynamics of a Gaussian wavepacket starting at either the energy of the transition state (upper frames, pertinent to thermal reactions) or four-times the energy of the diabatic crossover (lower frames, pertinent to photochemical processes) for characteristic points **A**, **E**, **H**, and **I** (see Table 1) as well as for molecules **0** ($FcPC_{60}$) at **5** (CT). The left frames show the diabatic potential-energy surfaces (red- L state, blue- R state) and the wavepacket's vibrational density resolved onto these states, while the right frames show the development of entanglement in the CA basis.

Alternatively, for entanglement perceived between diabatic states and the nuclear motion for both low-energy eigenfunctions and eigenfunctions near the transition state, the profile of the entanglement throughout the parameter space of the chemical model is distinctly different to those for the individual density-matrix elements considered in traditional analyses of chemical properties. Hence consideration of the entanglement reveals information in a unique and useable way. This is of particular significance as this type of entanglement may in principle be utilized in some quantum information technology. Further, the entanglement developed within reactive wavepackets for both thermal and photochemical reactions behaves in a simple way that could also possibly lead to technological exploitation.

## Appendix: Mathematical Symbols used

| Variable Class | Description | Variations |
|---|---|---|
| $Q$ | Generalized dimensionless normal coordinate describing the vibrational mode | $\pm Q_m$ – equilibrium values of the geometry in the uncoupled diabatic states<br>$Q_0$ – adiabatic equilibrium value on lower Born-Oppenheimer surface $\varepsilon_-^{BO}(Q)$<br>$Q_x$ - coordinate at which the adiabatic states are equal mixtures of the diabatic states<br>$Q_c$ - cusp diameter |
| $r$ | Coordinate of the coupled electron | |

| | | |
|---|---|---|
| $\mathbf{H}$ | Hamiltonian matrix | $\mathbf{H}^{CA}$ - electronic only, expressed in the diabatic (or "crude adiabatic") basis $\{L,R\}$<br>$\mathbf{H}^{BO}$ - electronic only, expressed equivalently in adiabatic ("Born-Oppenheimer") basis $\{-,+\}$ |
| $\Delta H$ , $\Delta P$ | Differences between the exact Hamiltonian and the BO Hamiltonian | $\Delta H^{DC}(Q)$ - diagonal correction, see Eqn. 8<br>$\Delta H^{FD}(Q) = \Delta P^{FD}(Q)\frac{\partial}{\partial Q}$ - first-derivative (momentum) correction, see Eqn. 8<br>$\Delta H^{SD}(Q)$ - second-derivative correction, see Eqn. 8 |
| $\lvert\phi(r,Q)\rangle$ | Electronic wavefunction at geometry $Q$ | $\lvert\phi_L^{CA}(r,Q_0)\rangle$ - electronic wavefunction of diabatic state $L$, coordinate independent<br>$\lvert\phi_R^{CA}(r,Q_0)\rangle$ - electronic wavefunction of diabatic state $R$, coordinate independent<br>$\lvert\phi_-^{BO}(r,Q)\rangle$ - electronic wavefunction of the ground adiabatic state<br>$\lvert\phi_+^{BO}(r,Q)\rangle$ - electronic wavefunction of the excited adiabatic state |
| $\lvert\chi_i(Q)\rangle$ | Vibrational basis | $\lvert\chi_i^L(Q)\rangle$, $\lvert\chi_i^R(Q)\rangle$ $i$-th harmonic-oscillator vibrational basis function for one of the diabatic states<br>$\lvert\chi_i^{\pm}(Q)\rangle$ $i$-th harmonic-oscillator vibrational basis function for one of the adiabatic states |
| $N$ | Basis set truncation | The number of harmonic-oscillator vibrational levels included per electronic state |
| $\lvert\psi(\mathrm{r},Q)\rangle$ | Vibronic eigenfunction | $\lvert\psi_j(\mathrm{r},Q)\rangle$ - *j-th* eigenfunctions of the full Hamiltonian matrix<br>$\lvert\psi_j'^{-}(\mathrm{r},Q)\rangle$ - *j-th* eigenfunctions of the ground Born-Oppenheimer state<br>$\lvert\psi_j'^{+}(\mathrm{r},Q)\rangle$ - *j-th* eigenfunctions of the excited Born-Oppenheimer state |
| $\varepsilon(Q), a(Q), b(Q)$ | Adiabatic state properties | $\varepsilon_-(Q)$ - energy of the ground Born-Oppenheimer adiabatic state<br>$\varepsilon_+(Q)$ - energy of the excited Born-Oppenheimer adiabatic state<br>$\varepsilon_-^{BH}(Q)$ - energy of the ground Born-Huang adiabatic state<br>$\varepsilon_+^{BH}(Q)$ - energy of the excited Born-Huang adiabatic state<br>$a(Q)$ - contribution of the $L$ diabatic state to the ground BO (same as BH) wavefunction<br>$b(Q)$ - contribution of the $R$ diabatic state to the ground BO (same as BH) wavefunction |
| $\varepsilon_j$ | Energy of the $j$-th vibronic level (0 ≡ lowest energy level) | $\varepsilon_j^{FC}$ - full calculation, only approximation is the vibrational basis-set truncation level $N$<br>$\varepsilon_j^{BO}$ - Born-Oppenheimer approximation<br>$\varepsilon_j^{BH}$ - Hamiltonian is BO plus DC (the Born-Huang approximation)<br>$\varepsilon_j^{FD}$ - Hamiltonian is BO plus FD<br>$\varepsilon_j^{SD}$ - Hamiltonian is BO plus SD |
| $\boldsymbol{\rho}$ | Reduced electronic density matrix | $\boldsymbol{\rho}_j$ - for vibronic eigenfunction $j$ in either the BO or CA electronic basis sets |
| $C$ | Vibronic eigenvectors of $\mathbf{H}$ | $C_{ij}^{-}$ coeff. of the $i$-th harmonic oscillator of the - state to the $j$-th vibronic wavefunction of $\mathbf{H}$<br>$C_{ij}^{+}$ coeff. of the $i$-th harmonic oscillator of the + state to the $j$-th vibronic wavefunction of $\mathbf{H}$ |
| $t$ | time | |
| $\lvert\Psi(\mathrm{r},Q;t)\rangle$ | Wavepacket | Time dependent wavepacket, initially of Gaussian shape at $t$=0. |
| $d_i(j)$ | Wavepacket composition | Specifies the time-dependent representation of a wavepacket in terms of the eigenfunctions of the approximate or exact Hamiltonian used |
| $\omega$ | Vibration frequency | $\omega$ - vibration frequency for the vibrational mode in both reactant and product diabatic surfaces |
| $J$ | Resonance integral | Electronic coupling between the two diabatic states, see Eqn. 1. |
| $\boldsymbol{\lambda}$ | Reorganisation energy | Difference between the vertical and relaxed excitation energies on the diabatic surfaces |
| $\Delta E$ | Electronic energy scale | $= \left(\lambda^2 + 4J^2\right)^{1/2}$ , used to scale the total energy of the interacting system, see Eqn. 17 |
| $E_0$ | Energy asymmetry | Energy difference (often taken as a free-energy difference) between the reactants and products |
| $\Delta E^{\dagger}$ | Activation energy | $\Delta E^{\dagger}$ - evaluated using the BH adiabatic approximation including the DC correction<br>$\Delta\Delta E^{\dagger}$ - the contribution to this actually coming from the DC correction |
| $S$ | Entanglement | Specified as the von Neumann entropy |

## Acknowledgments

We thank the Australian Research Council Discovery Projects scheme for funding, National Computational Infrastructure (NCI) for providing computational resources, and Profs. Meredith Jordan and Timothy Schmidt for helpful discussions.

**Notes and references**

*a: School of Chemistry, The University of Sydney, Sydney, NSW 2006 Australia*

*b: Department of Physics and Astronomy, University College London, Gower Street, London WC1E 6BT UK*

*c: School of Mathematics and Physics, The University of Queensland, Brisbane, QLD 4072 Australia*

*d: School of Molecular Biosciences, The University of Sydney, Sydney, NSW 2006 Australia*

*e: International Centre for Quantum and Molecular Structure, College of Sciences, Shanghai University, Shanghai 200444 China; Tel: 86-15618155341; E-mail: Jeffrey.Reimers@uts.edu.au*

*f: School of Mathematical and Physical Sciences, University of Technology Sydney, NSW 2007 Australia*

1. M. A. Nielsen and I. L. Chuang, *Quantum Computation and Quantum Information*, Cambridge University Press, New York, 2000.
2. A. P. Hines, C. M. Dawson, R. H. McKenzie and G. J. Milburn, *Phys. Rev. A*, 2004, **70**, 022303.
3. L. K. McKemmish, R. H. McKenzie, N. S. Hush and J. R. Reimers, *J. Chem. Phys.*, 2011, **135**, 244110/1.
4. A. J. Ferguson, P. A. Cain, D. A. Williams and G. A. D. Briggs, *Phys. Rev. A*, 2002, **65**, 034303.
5. S. Y. Cho and R. H. McKenzie, *Phys. Rev. A*, 2006, **73**, 012109.
6. R. Englman and T. Vértesi, *J. Chem. Phys.*, 2006, **125**, 064102.
7. R. Englman, *Phys. Lett. A*, 2007, **367**, 345.
8. T. Vértesi and R. Englman, *Phys. Rev. A*, 2007, **75**, 022315.
9. D. Wahyu Utami and A. A. Clerk, *Phys. Rev. A*, 2008, **78**, 042323.
10. B. Kinshuk and G. Gautam, *J. Phys. B: At., Mol. Opt. Phys.*, 2012, **45**, 045102.
11. T. Dereli, Y. Gul, P. Forn-Diaz and O. E. Mustecaplioglu, *Phys. Rev. A: At., Mol., Opt. Phys.*, 2012, **85**, 053841/1.
12. K. Banerjee and G. Gangopadhyay, *J. Phys. B: At., Mol. Opt. Phys.*, 2012, **45**, 045102.
13. H. Fujisaki, *Phys. Rev. A*, 2004, **70**, 012313.
14. F. Spano and L. Silvestri, *J. Chem. Phys.*, 2010, **132**, 094704.
15. L. Zhai and Y. Zheng, *Int. J. Quantum Chem.*, 2014.
16. Z. Huang and S. Kais, *Chem. Phys. Lett.*, 2005, **413**, 1.
17. T. Juhász and D. A. Mazziotti, *J. Chem. Phys.*, 2006, **125**, 174105.
18. K. Boguslawski, P. Tecmer, G. Barcza, O. r. Legeza and M. Reiher, *J. Chem. Theory Comput.*, 2013, **9**, 2959.
19. T. S. Hofer, *Frontiers in chemistry*, 2013, **1**.
20. Z. Huang, H. Wang and S. Kais, *J. Mod. Opt.*, 2006, **53**, 2543.
21. S. Kais, *Adv. Chem. Phys.*, 2007, **134**, 493.
22. M. Lombardi and A. Matzkin, *Phys. Rev. A*, 2006, **73**, 062335.
23. T. Maiolo, D. Fabio, L. Martina and G. Soliani, *Quantum Computers and Computing*, 2006, **6**, 43.
24. T. A. Maiolo, F. Della Sala, L. Martina and G. Soliani, *Theoretical and Mathematical Physics*, 2007, **152**, 1146.
25. L. Martina and G. Soliani, *arXiv preprint arXiv:0704.3130*, 2007.
26. O. Osenda, P. Serra and S. Kais, *International Journal of Quantum Information*, 2008, **6**, 303.
27. A. Ramšak, I. Sega and J. Jefferson, *Phys. Rev. A*, 2006, **74**, 010304.
28. H. Wang and S. Kais, *Isr. J. Chem.*, 2007, **47**, 59.
29. M. D. Shulman, O. E. Dial, S. P. Harvey, H. Bluhm, V. Umansky and A. Yacoby, *Science*, 2012, **336**, 202.
30. T. Westermann and U. Manthe, *J. Chem. Phys.*, 2012, **136**, 204116.
31. T. Westermann and U. Manthe, *J. Chem. Phys.*, 2012, **137**, 22A509.
32. Z. Bihary, D. R. Glenn, D. A. Lidar and V. Ara Apkarian, *Chem. Phys. Lett.*, 2002, **360**, 459.
33. R. de Vivie-Riedle and U. Troppmann, *Chem. Rev.*, 2007, **107**, 5082.
34. T. Cheng and A. Brown, *J. Chem. Phys.*, 2006, **124**, 034111.
35. K. Mishima and K. Yamashita, *Int. J. Quantum Chem.*, 2009, **109**, 1827.
36. C. M. Tesch and R. de Vivie-Riedle, *Phys. Rev. Lett.*, 2002, **89**, 157901.
37. L. Zhai and Y. Zheng, *Phys. Rev. A*, 2013, **88**, 012504.
38. X.-W. Hou, J. Huang and M.-F. Wan, *Phys. Rev. A*, 2012, **85**, 044501.
39. X. W. Hou, M. F. Wan and Z. Q. Ma, *Opt. Commun.*, 2008, **281**, 3587.
40. X.-W. Hou, J. Huang and M.-F. Wan, *Phys. Rev. A: At., Mol., Opt. Phys.*, 2012, **85**, 044501/1.
41. F. Hai-Ran, M. Xiang-Jia, L. Peng and Z. Yu-Jun, *Chinese Physics B*, 2014, **23**, 073301.
42. K. Mishima, K. Shioya and K. Yamashita, *Chem. Phys. Lett.*, 2007, **442**, 58.
43. K. Mishima and K. Yamashita, *Chem. Phys.*, 2010, **367**, 63.
44. K. Mishima and K. Yamashita, *Chem. Phys.*, 2009, **361**, 106.
45. T. Yoshino, S. Nishida, K. Sato, S. Nakazawa, R. D. Rahimi, K. Toyota, D. Shiomi, Y. Morita, M. Kitagawa and T. Takui, *J. Phys. Chem. Lett.*, 2011, **2**, 449.
46. K. Sato, S. Nakazawa, R. Rahimi, T. Ise, S. Nishida, T. Yoshino, N. Mori, K. Toyota, D. Shiomi, Y. Yakiyama, Y. Morita, M. Kitagawa, K. Nakasuji, M. Nakahara, H. Hara, P. Carl, P. Hofer and T. Takui, *J. Mater. Chem.*, 2009, **19**, 3739.
47. K. Sato, R. Rahimi, N. Mori, S. Nishida, K. Toyota, D. Shiomi, Y. Morita, A. Ueda, S. Suzuki, K. Furukawa, T. Nakamura, M. Kitagawa, K. Nakasuji, M. Nakahara, H. Hara, P. Carl, P. Höfer and T. Takui, *Physica E: Low-dimensional Systems and Nanostructures*, 2007, **40**, 363.
48. R. Rahimi, K. Sato, K. Furukawa, K. Toyota, D. Shiomi, T. Nakamura, M. Kitagawa and T. Takui, *International Journal of Quantum Information*, 2005, **3**, 197.
49. K. Sato, S. Nakazawa, S. Nishida, R. Rahimi, T. Yoshino, Y. Morita, K. Toyota, D. Shiomi, M. Kitagawa and T. Takui, in *EPR of Free Radicals in Solids II*, eds. A. Lund and M. Shiotani, Springer Netherlands, 2012, vol. 25, pp. 163.
50. C. H. Bennett and D. P. DiVincenzo, *Nature*, 2000, **404**, 247.
51. K. H. Marti and M. Reiher, *Phys. Chem. Chem. Phys.*, 2011, **13**, 6750.
52. T. Yonehara, K. Hanasaki and K. Takatsuka, *Chem. Rev.*, 2012, **112**, 499.
53. J. C. Tully, *J. Chem. Phys.*, 2012, **137**, 22A301.
54. K. Takatsuka, *J. Phys. Chem. A*, 2007, **111**, 10196.
55. M. Born and R. Oppenheimer, *Ann. Phys.*, 1927, **84**, 0457.
56. M. Born, *Nachr. Akad. Wiss. Gottingen, Math.-physik. Klasse IIa, Math.-physik.-chem. Abt.*, 1951, 1.
57. T. Azumi and K. Matsuzaki, *Photochem. Photobiol.*, 1977, **25**, 315.
58. B. T. Sutcliffe and R. G. Woolley, *J. Chem. Phys.*, 2012, **137**, 22A544.
59. J. R. Reimers, L. McKemmish, R. H. McKenzie and N. S. Hush, *Phys. Chem. Chem. Phys.*, 2015, **in press 10.1039/C5CP02238J**.
60. B. K. Kendrick, C. A. Mead and D. G. Truhlar, *Chem. Phys.*, 2002, **277**, 31.
61. A. W. Jasper, B. K. Kendrick, C. A. Mead and D. G. Truhlar, *Adv. Ser. Phys. Chem.*, 2004, **14**, 329.
62. M. D. Newton and N. Sutin, *Annu. Rev. Phys. Chem.*, 1984, **35**, 437.
63. T. Van Voorhis, T. Kowalczyk, B. Kaduk, L.-P. Wang, C.-L. Cheng and Q. Wu, *Annu. Rev. Phys. Chem.*, 2010, **61**, 149.
64. E. J. Barton, C. Chiu, S. Golpayegani, S. N. Yurchenko, J. Tennyson, D. J. Frohman and P. F. Bernath, *Mon. Not. R. Astron. Soc.*, 2014, **442**, 1821.
65. H. Rongsheng, L. Zijing and W. Kelin, *Physical Review B*, 2002, **65**, 174303.

66. J. R. Reimers, L. McKemmish, R. H. McKenzie and N. S. Hush, *Phys. Chem. Chem. Phys.*, 2015, **in press DOI:10.1039/C5CP02236C**.
67. J. R. Reimers, L. McKemmish, R. H. McKenzie and N. S. Hush, *Phys. Chem. Chem. Phys.*, 2015, **in press, DOI:10.1039/C5CP02237A**.
68. Z.-L. Cai and J. R. Reimers, *J. Phys. Chem. A*, 2000, **104**, 8389.
69. J. F. Stanton, *J. Chem. Phys.*, 2010, **133**, 174309.
70. J. R. Reimers, B. B. Wallace and N. S. Hush, *Phil. Trans. Roy. Soc. A*, 2008, **366**, 15.
71. N. S. Hush, in *Mechanistic Aspects of Inorganic Reactions*, eds. D. B. Rorabacher and J. F. Endicott., 1982, vol. 198, pp. 301.
72. S. Woitellier, J. P. Launay and C. W. Spangler, *Inorg. Chem.*, 1989, **28**, 758.
73. J. R. Reimers and N. S. Hush, *Inorg. Chem.*, 1990, **29**, 3686.
74. J. R. Reimers and N. S. Hush, *J. Chem. Phys.*, 2003, **119**, 3262.
75. J. R. Reimers and N. S. Hush, *J. Am. Chem. Soc.*, 2004, **126**, 4132.
76. D. Curiel, K. Ohkubo, J. R. Reimers, S. Fukuzumi and M. J. Crossley, *Phys. Chem. Chem. Phys.*, 2007, **9**, 5260.
77. S.-H. Lee, A. G. Larsen, K. Ohkubo, Z.-L. Cai, J. R. Reimers, S. Fukuzumi and M. J. Crossley, *Chem. Sci.*, 2011, **3**, 257.
78. M. Brinkmann, G. Gadret, M. Muccini, C. Taliani, N. Masciocchi and A. Sironi, *J. Am. Chem. Soc.*, 2000, **122**, 5147.
79. S. Yin, L. Li, Y. Yang and J. R. Reimers, *J. Phys. Chem. C*, 2012, **116**, 14826.
80. E. B. D. Wilson, J. C; Cross, Paul C., *Molecular Vibrations: The Theory of Infrared and Raman Vibrational Spectra*, McGraw-Hill Book Company, New York, 1955.
81. M. Born and K. Huang, *Dynamical Theory of Crystal Lattices*, Clarendon, Oxford, 1954.
82. R. Horodecki, P. Horodecki, M. Horodecki and K. Horodecki, *Rev. Mod. Phys.*, 2009, **81**, 865.
83. M. Reis, M. O. T. Cunha, A. C. Oliveira and M. C. Nemes, *Phys. Lett. A*, 2005, **344**, 164.
84. L. D. Landau, *Z. Phys. Sowjetunion*, 1932, **2**, 46.
85. C. Zener, *Proc. R. Soc. London, Ser. A*, 1932, **137**, 696.
86. D. N. Beratan and J. J. Hopfield, *J. Chem. Phys.*, 1984, **81**, 5753.
87. P. T. Saunders, *An introduction to catastrophe theory*, Cambridge University Press, Cambridge, 1980.
88. F. Xu, *Z. Phys. Chem.*, 1990, **166**, 79.
89. X. Krokidis, B. Silvi, C. Dezarnaud-Dandine and A. Sevin, *New J. Chem.*, 1998, **22**, 1341.
90. D. J. Wales, *Science*, 2001, **293**, 2067.

## TOC graphic

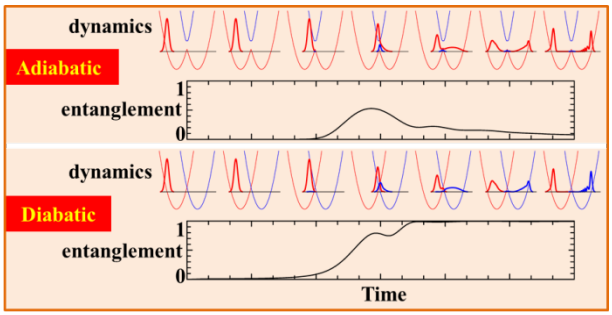


NOVELTY STATEMENT Entanglement in the diabatic basis produces useful quantum information whilst that in the adiabatic basis tells how good is the Born-Oppenheimer approximation.